Project Reports

Hypothesis 1: The forced, two-gyre vorticity wave response of the lake to episodic wind events, occasionally modified by stratification, is a major mechanism for nearshore-offshore transport of particulate matter and associated constituents in the Great Lakes.

What have we learned so far? (as of 11/99)

- The longshore convergence associated with the forced, two-gyre vorticity wave is apparent in the first set of current meter and drifter measurements from 1997-98.

- Preliminary hydrodynamic model results indicate qualitative agreement with observed currents and sediment deposition patterns.

- Offshore flow and resulting sediment resuspension and transport are sensitive to local meteorology.

Results

- HF Radar Measurements
- Remote Sensing.
- HOC fluxes.
- Meteorological modeling.
- OSU products and sediment modeling.
- GLERL hydrodynamic modeling and sediment transport.

Future Plans

- Coupled hydrodynamic/ sediment dynamics modeling system (GLERL/OSU).
- Further biological model case studies (March-April, 1998 & 1999).
- Meteorological model case studies.

Reports (9/00):

Meteorological Modeling Program -- P. Roebber

Retrospective Analysis: Measuring the Historical Magnitude of Turbidity Plumes Using Archived Remotely Sensed Imagery -- J.W. Budd, W.C. Kerfoot, R.P. Stumpf, and Katherine Strojny

HF Radar Observations of Currents, Winds and Waves -- John F. Vesecky, Lorelle A. Meadows, Calvin C. Teague, Pete Hansen, Jeff Paduan, Dan Fernandez, and Yolanda Fernandez

The Impact of Episodic Events on Nearshore-offshore Transport in the Great Lakes: Physical Oceanography -- J.H. Saylor, G.S. Miller, and M. J. McCormick, Canadian Colleagues: C.R. Murthy, R. Rao, K. Miners, F. Chiocchio, and J. Bull

The Impact of Episodic Events on Nearshore-offshore Transport in the Great Lakes: Hydrodynamic Modeling Program -- David J. Schwab and Dmitry Beletsky

Meteorological Modeling Program

Paul J. Roebber, University of Wisconsin – Milwaukee.

Objectives:

1. Accurately describe the overwater wind field during storms (including fine-scale variations) in order to assess the importance of wind-induced currents and waves in initiating and maintaining resuspension events.
2. Address the question as to whether resuspension events represent a response to the aggregate effects of a season of individual storm events or an episodic response to a single large storm event.

Approach

- Configure mesoscale meteorological model for realtime and hindcast simulations of events;
- For specific resuspension events, generate hindcast "control" simulations that well reproduce the observed meteorological and lake circulations;
- Test response to fine-scale storm details by providing meteorological data during resuspension at 6 km grid spacing;
- Place resuspension events into historical context, by investigating (with Dave Schwab) the meteorological and oceanographic aspects of prior events.

Results

- Clear evidence from frequency and magnitude of resuspension events during field program that they are an episodic response to storm events;
- Fine-scale features, such as the wind vortex of 11 March 1998, play a role in lake circulation and the transport of resuspended sediment;
- Mesoscale model data provide improved input to hydrodynamic models

Research Products (Publications, conference papers and presentations)

Roebber, P.J. and M.G. Gehring, 2000: Realtime prediction of the lake breeze on the western shore of Lake Michigan. *Wea. Forecasting*, 15, 298-312.

Roebber, P.J., 2000: The use of storm-scale resolution NWP for operational forecasting of atmospheric convection. *International Conference on Scientific Computing*, Milwaukee, WI, 25-27 May 2000.

Roebber, P.J., 1999: The role of Lake Michigan in modulating upstream weather conditions: experience with realtime forecasts using MM5 in warm and cold seasons and priorities for future model development. *Proceedings of the 9th Penn State/NCAR MM5 Users' Workshop*, 23-25 June 1999, Boulder, CO.

Beletsky, D., D.J. Schwab, P.J. Roebber and J. Lou, 1999: Hydrodynamic modeling for the 1998 Lake Michigan coastal turbidity plume event. *Proceedings of the 6th International Conference on Estuarine and Coastal Modeling*. 3-5 November 1999, New Orleans, LA

Collaborators

Schwab (hydrodynamic modeling and historical investigation of prior events) and Beletsky (hydrodynamic modeling)

Retrospective Analysis: Measuring the Historical Magnitude of Turbidity Plumes Using Archived Remotely Sensed Imagery

J.W. Budd[1], W. C. Kerfoot[2], R.P. Stumpf[3], Katherine Strojny[2]
[1]MTU/Geological Engineering & Sciences, [2]MTU/Biological Sciences, [3]NOAA/NOS

Goal:
The overall goal is to analyze and interpret all available operational remotely sensed imagery of southern Lake Michigan using state-of-the art image processing techniques.

Objectives:
1. analyze and archive historical Advanced Very High Resolution Radiometer (AVHRR) lake surface temperature (LST) and remote sensing reflectance (R_{rs}) imagery.
2. provide the first-ever chlorophyll (C_{SAT}) and R_{rs} (related to turbidity) estimates from the Sea-viewing Wide-Field-of-View Sensor (SeaWiFS) imagery using a revised atmospheric correction procedure developed by Stumpf et al.
3. create year-long, uninterrupted time-series SeaWiFS imagery using a statistically-based time-space interpolation procedure.
4. create multi-sensor visualizations of physical (AVHRR LST) and particle (SeaWiFS C_{SAT}, R_{rs}) data.
5. validate the satellite-derived water parameters with in situ data from intensive field surveys at sampling locations.
6. support modeling groups' efforts (Schwab et al., Chen et al.) by providing synoptic satellite water parameters for model experiments.

Approach:
* All available AVHRR (1989 to present) and SeaWiFS (1997 to present) imagery were processed and are being analyzed. Geotiff images are posted at http://www.geo.mtu.edu/great_lakes/lakersi/cgi-bin/seawifs.cgi and http://www.geo.mtu.edu/great_lakes/lakersi/cgi-bin/avhrr.cgi.
* Multi-sensor visualization techniques were employed in comparative studies of the time, duration and spatial extent of episodic events using statistically-based interpolation techniques, an edge detection algorithm (Diehl and Budd, in review) and data fusion of simultaneously-acquired remotely sensed data.
* A digital bathymetry model was coupled with SeaWiFS sediment maps (as R_{rs}) to obtain instantaneous estimates of total mass of resuspended sediments in southern L. Michigan.
* Comparisons of ship-based chl-a and TSS with satellite-derived parameters provide validation of SeaWiFS C_{SAT} and R_{rs}.

Selected Results:
* Historical AVHRR Rrs imagery from 1992 to 1999 reveal that episodic resuspension events occur throughout the fall, winter and spring months from from September to the end of April.
* Distinct horizontal temperature gradients from nearshore to offshore were observed in late March and April in Lake Michigan. The presense of a thermal bar indicated a transition zone between nearshore (warmer) from offshore (colder) waters.
* Using SeaWiFS chlorophyll and sediment maps of southern Lake Michigan in late spring, we identified two chlorophyll maxima in nearshore and offshore waters, which were separated by the thermal bar. Whereas the nearshore chlorophyll maxima was strongly coupled to resuspended sediment, the offshore chlorophyll maxima was not.
* Calculations of daily total mass of sediment during the spring plume event of 1998 range from 2.8×10^9 kg (Fig. 1).

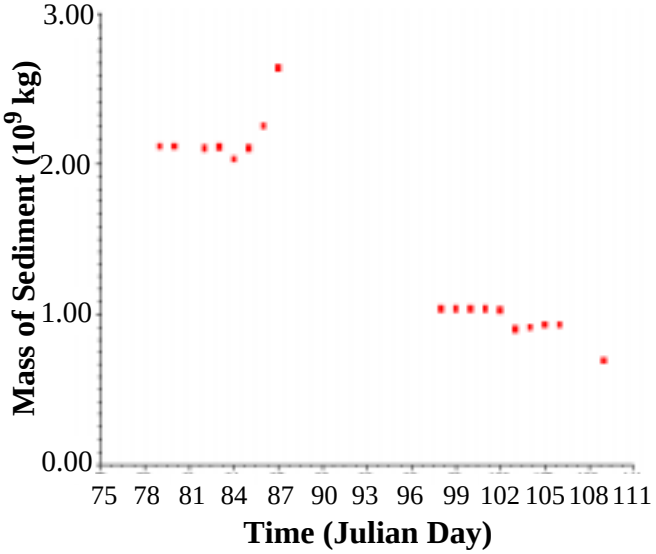

Fig. 1. Total mass of sediment/day in southern L. Michigan during spring 1998 based on SeaWiFS interpolated TSS estimates and 1 km^2 bathymetry contours. Gaps in data represent periods when clouds precluded interpolation.

Geographic window sizes applied to remote-sensing sea-surface temperature front detection

Scott F. Diehl, Judith Wells Budd, and more to come

Michigan Technological University

Houghton, Michigan 49931

Abstract:

This paper investigates the effects of using a geographic window size with an existing edge detection technique. A geographic window is one whose size is not constant, but is determined by the correlation of the data surrounding the window's central point. Using this approach instead of a fixed window size, the investigation window is optimized for all of the image, providing more reliable detection of edges within the window. The new algorithm was run on several SST images from southern Lake Michigan and compared to runs of the original algorithm and a modification of the original algorithm optimized for this region. The results show that the geographic window improves edge detection most in the near-shore regions, and to a lesser extent in the off-shore regions.

Introduction:

The location and identification of sea-surface temperature fronts in satellite-derived imagery of lakes and oceans is important for understanding many physical and biological processes that

occur in these regions. Subjective human analysis of these images can detect edges corresponding to thermal fronts that indicate the existence of currents, upwellings, eddies, and various other phenomena. The frequency, size, and duration of these events can then be studied in time series of imagery to gain further understanding of these occurrences. However, using human analysis on a large number of satellite images is a time-consuming process. This type of approach also introduces unnecessary bias into the analysis, based on inconsistencies in human processing capabilities. An automated objective edge detection algorithm, using consistent statistical measures on each image, is a more reliable and less time consuming solution than human analysis.

There are currently many different algorithms that have been developed for automated edge detection. Many of the more commonly used methods, such as the Sobel operator, the gradient technique, and the mathematical Laplacian are discussed by Davis (1975) and Levialdi (1981). Holyer and Peckinpaugh (1989) chose not to use these operators as they are too sensitive to local noise and weak gradients, and developed their own algorithm, called the cluster-shade technique. Cayula and Cornillon (1992) developed a single-image edge detection algorithm (SIED), which uses overlapping windows to investigate the statistical likelihood of an edge existing in each window by performing a histogram analysis on the SST field. The cluster-shade technique and SIED were compared in a correspondence between the authors, and the latter algorithm was found to have superior performance (Cayula et al, 1991). A modification of this algorithm was later applied to the Great Lakes region when Ullman et al. (1998) used Cayula and Cornillon's (1995) multi-image edge detection (MIED) algorithm, to conduct a study of temperature fronts in the Great Lakes.

A possible improvement to the algorithms was suggested by Franklin et al (1996). Although originally planned for applications with satellite image texture analysis, a “geographic window” was suggested to be used to improve satellite image edge detection. A geographic window is one whose size is determined by the correlation of the data surrounding the window’s central point. Thus, the window size would be approximately optimal for all points of investigation, rather than optimal in some regions and suboptimal for other regions.

This paper investigates the application of a geographic window in edge detection to determine whether this method offers improvements over fixed window analysis techniques. Since Cayula and Cornillon’s (1992) single image edge detection (SIED) has distinct advantages over previous algorithms (Cayula et al., 1991), this algorithm was chosen for the study. Applying geographic window analysis to SIED, the resulting modification is used to provide a comparison with the fixed-window approaches used by Ullman et al. (1998).

Methods:

Overview of algorithm:

The algorithm presented in this paper, the Variable Window Single Image Edge Detection (VW-SIED), is concerned with the location of sea-surface temperature fronts in water bodies such as the Great Lakes. VW-SIED is a modified version of Cayula and Cornillon’s (1992) Single Image Edge Detection (SIED) algorithm. The original SIED algorithm is a six-step process (illustrated in figure 1) involving cloud detection (steps 1-3), histogram analysis (step 4) and application of a cohesion algorithm (step 5) using a fixed investigation window size, and a contour following algorithm (step 6).

The three-step cloud detection algorithm locates and then masks clouds in the image. These steps include image thresholding, histogram analyses and correlation algorithms. After the clouds have been located and masked, the “window-level” edge detection step begins. The SST image is divided up into overlapping windows of fixed size. Each window of the image is tested for the likelihood of an edge being present with a histogram analysis (step 4) followed by a cohesion test (step 5). If both of these tests are positive, then an edge is marked along the border of the two populations. The “window-level” edge detection is followed by a “local-level” edge detection stage (step 6). This stage includes a contour following procedure that uses gradient information to extend and connect isolated edges, as well as to eliminate insignificant edges (Cayula and Cornillon, 1992).

Modifications to SIED:

Franklin et al (1996) suggested that the use of a "geographic window", whose size depends on the correlation of the surrounding data, would improve edge-detection techniques. VW-SIED adapts this idea to focus on improving the “window-level” processing of SIED. This is meant to rectify the problem of a fixed window size being optimal for one part of an image, but suboptimal for another.

Geographic window size determination (step 3A):

The size of each geographic window in VW-SIED is based on a statistical measure of the surrounding data called the “semivariance” (Davis, 1973). Semivariance is a representation of the spatial correlation between points of data separated by specific lags (the distance between two points), and the semivariogram is the plot of the semivariance against the lag. In a typical semivariogram in which a spatial relationship exists in the data, the semivariance will increase as the

lag between points increases. The lag at which the semivariance reaches its maximum and no longer increases steadily is called the range, and indicates the distance at which the data are no longer related (Davis, 1973). An example of a semivariogram is shown in Figure 2.

The semivariance at lag h is calculated by summing the squared differences of the values of all data pairs (X_i and X_{i+h}) along a line of length n.

$$\gamma(h) = \sum_{i}^{n-h} \frac{(X_i - X_{(i+h)})^2}{2n}$$

This value is calculated separately for each h along a line centering on the point of investigation along a horizontal and vertical orientation. Since the semivariogram indicates that the data are no longer related at distances greater than its range (Davis, 1973), the range of the semivariograms can be used as guidelines for window size (Franklin et al, 1996). VW-SIED uses the ranges of the horizontal and vertical semivariograms for the x and y dimensions of the investigation window, respectively. Thus, each window size is a rectangle whose dimensions are based on the correlation of the data surrounding its central point. The window-determination process is graphically represented in Figure 2.

Cayula and Cornillon (1992) overlapped the windows in their algorithm, but since the window size is now variable, VW-SIED must have a method to overlap its investigation windows without overcrowding them. If windows are placed too frequently, multiple fronts will be detected where only one exists due to the small differences in each window. However, if windows are placed with no overlap at all, fronts located near the boundaries of each window may be missed. Thus, in order to appropriately overlap its windows, VW-SIED keeps track of which pixels have been pre-

viously investigated, and starts each new window investigation at the first unvisited pixel not included in a previous analysis. This causes each window to overlap the previous window's investigation by half its size in each direction, allowing for sufficient overlap to detect fronts near the boundaries of windows without risking edge multiplicity.

Window investigation (step 4 and 5):

After the window size is determined, this window is then investigated for the likelihood of an edge existing. A histogram analysis is performed on the data to locate the edge. If the histogram is bimodal, then it is very likely that an edge will exist. The histogram procedure designed by Cayula and Cornillon (1992) exhaustively investigates each possible threshold value (0-255 in 8 bit data), finds the optimal threshold to divide the histogram into two well defined populations, and then examines the ratio of the between-cluster variance to the within-cluster variance. If this ratio is greater than a value of 0.7, the test is passed. However, the criterion value suggested by Cayula and Cornillon (1992) was not selective enough when detecting fronts in the Great Lakes. In a previous study of thermal fronts in the Great Lakes (Ullman et al, 1998), a criterion value of 0.76 was found to be optimal for this region. We chose this value for use in this study.

Whenever step 4 indicates the existence of two populations, step 5 is then used to test the window to determine whether the two populations are spatially distinct. The neighbors of each pixel within the window are examined to determine whether or not they are in the same population. This comparison yields three cohesion ratios, C_1, C_2, and C:

$$C_1 = R_1 / T_1$$

$$C_2 = R_2 / T_2$$

$$C = (R_1 + R_2) / (T_1 + T_2)$$

Where C_1, C_2, and C are the cohesion ratios for the first, second, and both populations, respectively, T_1 and T_2 are the total number of comparisons between center pixels in population 1 or 2, respectively, and neighboring pixels. R_1 and R_2 are the number of comparisons between center pixels in population 1 or 2, respectively, and neighbor pixels that are in the same population. Cayula and Cornillon (1992) suggest minimum values of 0.90 for C_1 and C_2 and 0.92 for C. However, the derivations for these threshold values decrease by a factor that is inversely proportional to the window size:

$$C_? = 1.00 - (1/w) - 2\ P(error)$$

Where w is the window size, and P(error) is the maximum tolerable probability of error. These values assume a window size of 32x32 pixels is used, and a P(error) of 0.025 for C and 0.035 for C_1 and C_2. Since VW-SIED utilizes variable window sizes, w must be replaced by the window size used in that particular investigation. Since the window is not a square, however, the average of the x and y dimensions of the window is used instead. If the cohesion ratios are greater than this threshold, then the populations are determined to be spatially compact enough to indicate the existence of two statistically distinct populations of pixels.

If both the histogram and cohesion tests are affirmative for a particular window, the existence of a front is verified, and any pixel bordering another pixel from the other population is marked as an edge. In order to avoid doubly thick edges, only the bottom and right neighbors of each pixel is investigated. The entire process beginning with the window size determination is then repeated

for the next unvisited pixel until there are no new pixels, and thus the whole image has been investigated. These edges are then overlaid onto the original image and output to a file.

Imagery Test Runs:

The effectiveness of VW-SIED was tested using twelve AVHRR (Advanced Very High Resolution Radiometer) SST images. These images are from the springtime of 1998, 1999, and 2000 in southern Lake Michigan. This is an excellent period to detect thermal fronts, as the thermal structure of the lake is changing rapidly with the transition from wintertime temperature that are basically homothermal (at below four degrees Celcius) to springtime temperatures, characterized by the development of a thermal bar (shore parallel density maxima at four degrees Celcius) and its movement offshore.

To provide a basis of comparison, VW-SIED was run on each test image, as well as the original SIED algorithm, using Ullman's (1998) settings of a 32x32 pixel window (UL-SIED). A 15x15 pixel window was found to be more optimal for southern Lake Michigan, so an algorithm using optimized settings (OP-SIED) was also run. Since VW-SIED is an improvement only on the window-level processing of SIED (steps 4 and 5), the local-level contour following (step 6) is skipped to facilitate a direct comparison of the improvement in the window-level processing.

Results:

Maximum Lag Determination:

Before running VW-SIED a maximum lag value for the semivariograms had to be determined. This value is the length of the line along which the semivariance is calculated on both the x and y axes around a central point. Due to factors such as local noise, the semivariogram does not always have a well defined range, so dynamically judging when to stop analysis is a difficult matter. Placing an absolute limit on the size of the investigation fixes the number of calculations needed to obtain a reliable estimate of the range at a reasonable value. According to a study of semivariance in remote sensing, the maximum lag should be between one-fifth and one-third of the total lags (Curran, 1988). The images of southern Lake Michigan that were tested were 153 pixels wide and 268 pixels long (including land pixels). These land values, however, should not be used for the consideration of the maximum lags because this study is concerned with the temperature fronts on the lake surface itself, not with those on the land. The dimensions of the lake surface itself were used to calculate the maximum lags, and since the lake is longer than it is wide, the width is the limiting factor in this calculation. The width of southern Lake Michigan varies from a minimum of about 60 pixels wide to a maximum of about 110 pixels wide. Using this information, a value of 21 was chosen for the maximum lag value of VW-SIED.

Optimization of UL-SIED:

The results reveal that the UL-SIED settings were suboptimal for the southern Lake Michigan subset. Figure 3 shows several examples of UL-SIED completely failing to detect many of the important fronts, including those that can be detected by subjective human analysis in an image,

such as the fronts between warm coastal water and colder off-coast water on 4/17/1998 and 4/25/2000. This is due to the close proximity of the SST fronts to the land/water boundary, where a more heavily weighted edge exists. A 32x32 pixel window is too large to detect many of these near-shore fronts, as well as fronts that are in close proximity to other fronts, due to the algorithm's ability to evaluate a window containing only two populations. We found a more optimal window size for this region to be a 15x15 pixel window (OP-SIED), which is large enough to provide reliable statistical information while still being small enough to have the sensitivity to detect many near-shore temperature fronts.

Comparison of Edge Detection Results:

VW-SIED offers a more complete detection of the SST fronts, especially those in the near-shore regions. In the 3/12/1998 image, UL-SIED fails to detect a front in the western part of the lake, while OP-SIED poorly detects the southern front. VW-SIED detects all of these features well. This image demonstrates how a fixed window size can be optimal for some areas yet suboptimal for others, and how a variable window can fix this problem. The 3/21/1998 image shows UL-SIED failing in many places where OP-SIED and VW-SIED both indicate the presence of fronts. The image from 4/17/1998 is an excellent example of the impact of window size on the detection of coastal features. UL-SIED detects no near-coast fronts, OP-SIED reveals some, but not many, while VW-SIED shows many layers of near-shore thermal structure. Similar occurrences are observed in 4/27/1999, 4/29/1999, and 4/25/2000. The same can be said for 4/18/1998 and 4/29/1999, except that UL-SIED does detect the near-shore fronts in some regions fairly well.

In the images acquired on 3/14/1999, 3/29/1999, and 3/05/2000, similar results for the three algorithms were obtained, yet it appears that UL-SIED detects the mid-lake fronts better than the other

two. This difference is an artifact of UL-SIED's window size, rather than the result of a failure in VW-SIED. UL-SIED assimilates these front segments into an evaluation of its relatively large 32x32 window, and then traces the edge along the border of the two populations that are detected. These are detected due to two well-defined populations that exist in another portion of the window that weight the statistics for the rest of the window towards the indication of an edge. An investigation of the SST gradient in the disputed region shows that the pixel value differs by only 1 count. VW-SIED, however, includes these front-free segments in a separate window, and their histogram analysis indicates that no edge is present. Thus, some of the segments detected in UL-SIED are actually artifacts introduced by an overly large window.

Another inherent problem of a fixed window algorithm is that it can detect only one or two populations within a window. If there are three or more populations in a window, the statistics will be confused and the tests will most likely fail. This type of occurance can be shown in the 4/17/1998, 4/29/1999, and 3/05/2000 imagery. This problem is especially of concern in the detection of near-coastal fronts, where three populations are in close proximity-- land, near-shore water, and off-shore water. Large windows have a good chance of encountering all three populations in one investigation, and this could cause the algorithm to fail. However, SIED uses a land-mask to avoid this problem-- pixels marked as land are not included in the histogram analysis, thus reducing the three populations to two. Large windows still have problems in this region despite this precaution, because the near-shore populations are usually very thin regions compared to the off-shore region that cannot impact the histogram significantly enough to indicate an edge. Smaller windows have less chance of encountering this problem, but smaller windows are sub-optimal for detecting the larger populations that exist in the off-shore features. VW-SIED's variable window

provides a solution to this problem, offering window sizes that are optimal for both near-shore and off-shore areas.

Semivariogram analysis:

In order to understand why VW-SIED accomplishes better near-coast and near-front edge detection, it is necessary to investigate the semivariogram data. Pseudo-color imagery of the window sizes acquired from the range of the semivariograms of each pixel are shown in Figure 4 for both the x and y sizes. Around an off-shore vertical edge, the range of the x semivariogram increases to a local maxima (as for a horizontal edge and the range of the y semivariogram) on the edge itself. The result of this is that the window that lies exactly on an edge pixel will have a large window of investigation (shown in Figure 4 to be usually between 11 and 15 pixels), but as the point of investigation moves away from the edge, the window size becomes smaller, reducing the chance of investigating that front in a different window whose center is further away from the front (and thus more likely to include a second front and confuse the statistics).

VW-SIED behaves slightly differently in the near-shore regions. The local maxima of the x or y range is not encountered on the corresponding horizontal or vertical edge pixel itself, but rather between the land/water edge and the near-shore SST front. This is due to the fact that the data are decreasing steadily throughout most of the transect at these points, and thus the semivariogram will indicate a high level of correlation. This is also positive, in that the maximum value in between the two edges is always only enough to investigate the area between the two edges (and not include the edges themselves) due to the fact that the data on either side of the edges are relatively constant (land values and off-shore values). As the investigation moves away from each of the two edges, the range of the semivariance reduces only slightly, causing the window to incorpo-

rate only one of the two fronts. Thus, a window will most likely never be exposed to more than one front at a time. Since the statistics involved in SIED assume that there will only be two populations present in a window, this results in more reliable calculations in areas where fronts are in close proximity to each other.

Processing Time:

The average processing time for VW-SIED is 20.77 seconds for the southern Lake Michigan images run on a Sun Ultrasparc 60. UL-SIED and OP-SIED took a considerably shorter time to run, taking 5.07 seconds and 7.67 seconds on average, respectively. This difference is caused by the semivariogram investigation of VW-SIED adding more investigations per pixel.

Discussion:

The edge-detection algorithm presented in this article was used to investigate the effect of a variable "geographic" window size on the performance of a previously published edge-detection algorithm developed by Cayula and Cornillon (1992). The performance of the original is improved especially in areas with greater than two populations. In these areas, UL-SIED and OP-SIED failed consistently because the fixed window overlapped three different populations of pixels, and since the algorithm cannot handle more than two populations in any window, this caused it to fail. The variable windows help to alleviate this problem by customizing the window size to prevent more than two populations from being present in any one window. The variable window

approach presented here also improves the detection of fronts in other regions by reducing the presence of edges that are actually artifacts introduced by large windows.

The trade-off for this increased performance is evident in the processing time required by the algorithm. For the southern Lake Michigan subset, it took 3-4 times as long to operate as either of the other two settings of SIED. This is a minor consideration for those with unlimited access to high-powered computers, since the algorithm could be run overnight or on the weekends if it were needed to be run on many images or images of large sizes. But for those without these capabilities, OP-SIED presents a less CPU-time intensive solution, which still offers reliable results for this subset. Also, in an image that contains relatively few or unimportant near-shore regions, such as imagery obtained for the open ocean or a Lake Superior subset of the Great Lakes, VW-SIED may offer little improvement, making the extra processing time unnecessary.

The increased performance of VW-SIED for near-shore temperature fronts will allow for more reliable investigations into phenomena relating to these fronts. For example, high primary productivity often occurs near fronts (Mortimer 1988), and a data fusion process involving SST fronts output by VW-SIED and chlorophyll imagery derived from SeaWiFS could be used to illustrate the co-occurrence of biological and physical fronts in southern Lake Michigan. However, without the increased performance of VW-SIED, many of the products could be misleading, especially for near-shore regions, which are the most important areas for understanding coastal processes.

An improvement to VW-SIED could be gained by implementing a multi-image version (VW-MIED) of this algorithm. Cayula and Cornillon (1995) used this method to improve their original SIED algorithm, using the assumption that fronts are correlated not only in space, but also in time.

The multi-image edge detection technique involves an investigation of images within a certain time-frame to identify persistent fronts, and then using these fronts to help the detection of weak contours or contours in cloud-contaminated regions in each image within the time-frame. The development and application of a VW-MIED could yield additional benefits over VW-SIED.

References:

Cayula, J.-F., and P. Cornillon, 1992, Edge detection algorithm for SST images: J. Atmos Oceanic Technol., 9, pp. 67-80.

Cayula, J.-F., and P. Cornillon, 1995, Multi-image edge detection for SST images: J. Atmos Oceanic Technol., 12, pp. 821-829.

Cayula, J.-F., and P. Cornillon, R. J. Holyer, and S. H. Peckinpaugh, 1991, Comparative study of two recent algorithms designed to process sea-surface temperature fields: IEEE Trans. on Geosci. and Remote-Sens., GE-29, pp. 175-177.

Curran, P., 1988, The semivariogram in remote sensing: an introduction: Remote Sensing Environment, v. 24, pp. 493-507.

Davis, J. C., 1973, Statistics and data analysis in geology: John Wiley & Sons, Inc., New York, pp. 239-248.

Davis, L. S., 1975, A survey of edge detection techniques: Comput. Graph. Image Proc., vol. 4, pp. 248-270.

Franklin, S. E., Wulder, M. A., and Lavigne, M. B., 1996, Automated derivation of geographic window sizes for use in remote sensing digital image texture analysis: Computers and Geosci., 6, pp. 665-673.

Holyer, R. J., and Peckinpaugh, S. H., 1989, Edge detection applied to satellite imagery of the ocean: IEEE Trans. Geosci. Remote Sens., GE-27, pp. 46-56.

Levialdi, S., 1981, Finding the edge: Digital Image Processing, J.C. Simon and R.M. Haralick, Eds. Reidel Publishing Company, pp. 105-148.

Mortimer, C. H., 1988, Discoveries and testable hypotheses arising from Coastal Zone Color Scanner imagery of southern Lake Michigan: Limnol. Oceanogr., 33, pp. 203-226.

PCI Inc., 1994, EASI/PACE Image analysis system manual, version 5.3: PCI Incorporated, Richmond Hill, Ontario, variously paged.

Ullman, D., Brown, J., Cornillon, P., and Mavor, T., 1998, Surface temperature fronts in the Great Lakes: J. Great Lakes Res., 24, pp. 753-775.

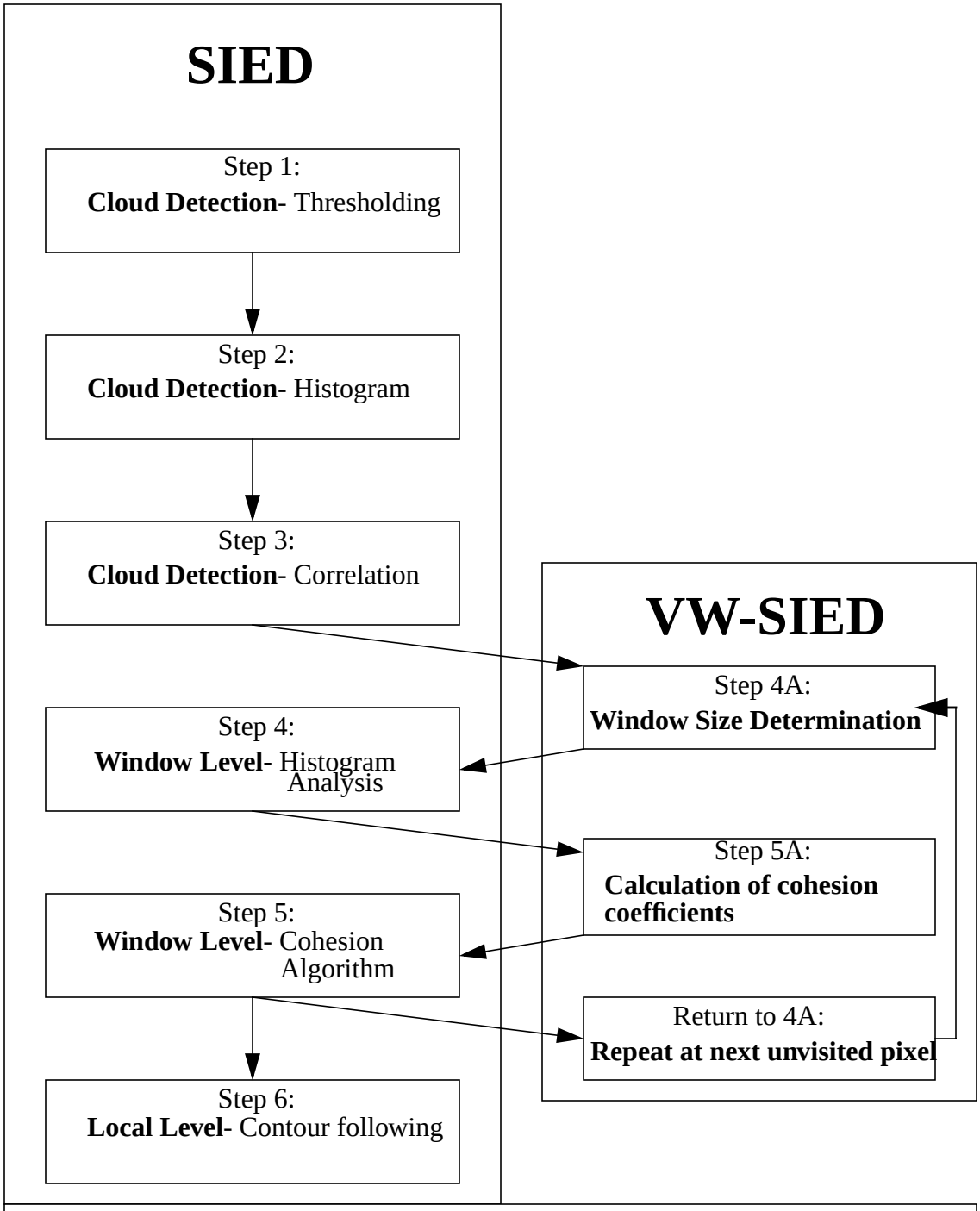

Fig 1. Flowchart of the SIED algorithm detailing the changes that are made for the VW-SIED algorithm.

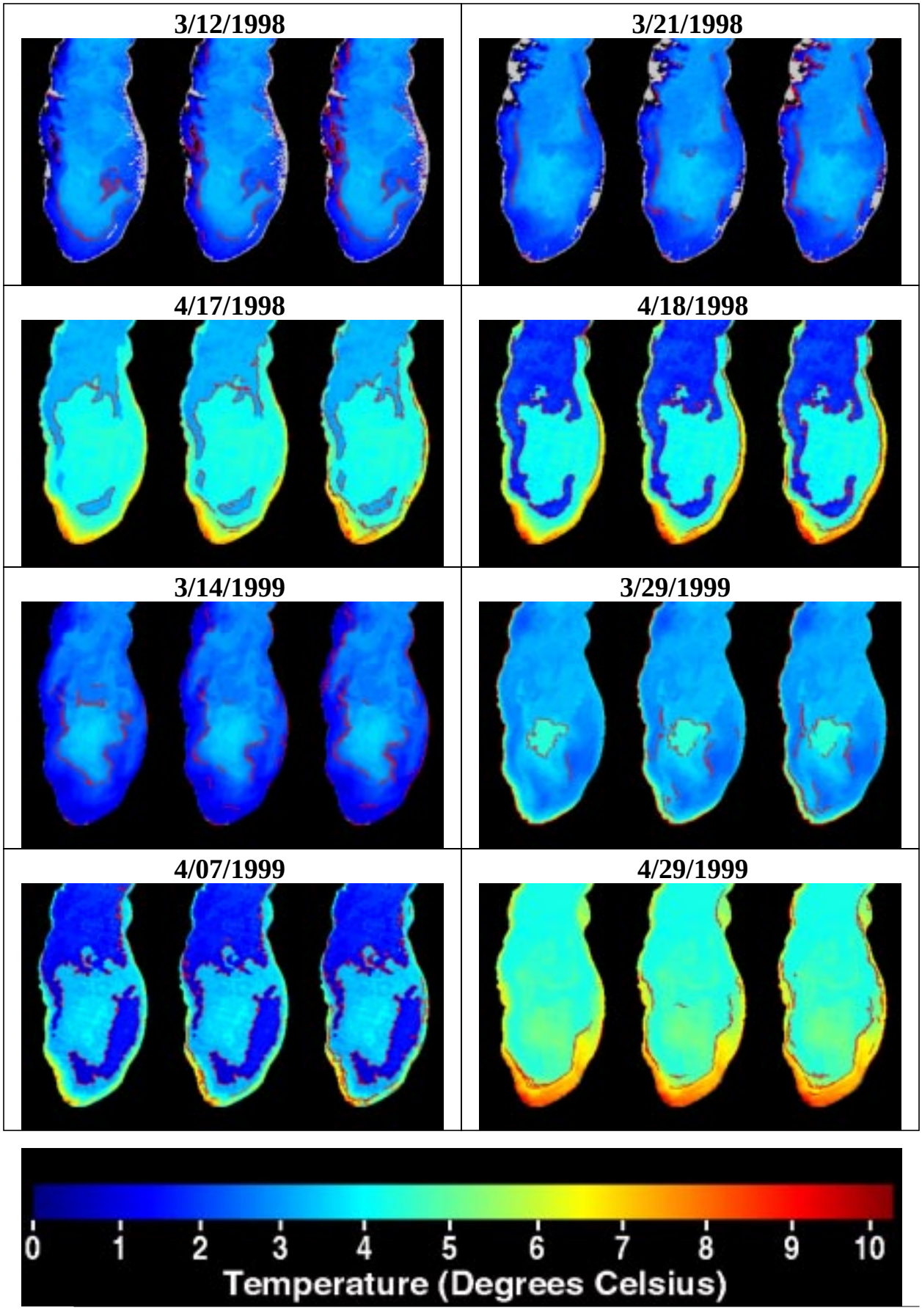
3/12/1998
3/21/1998
4/17/1998
4/18/1998
3/14/1999
3/29/1999
4/07/1999
4/29/1999
0
1
2
3
4
5
6
7
8
9
10
Temperature (Degrees Celsius)

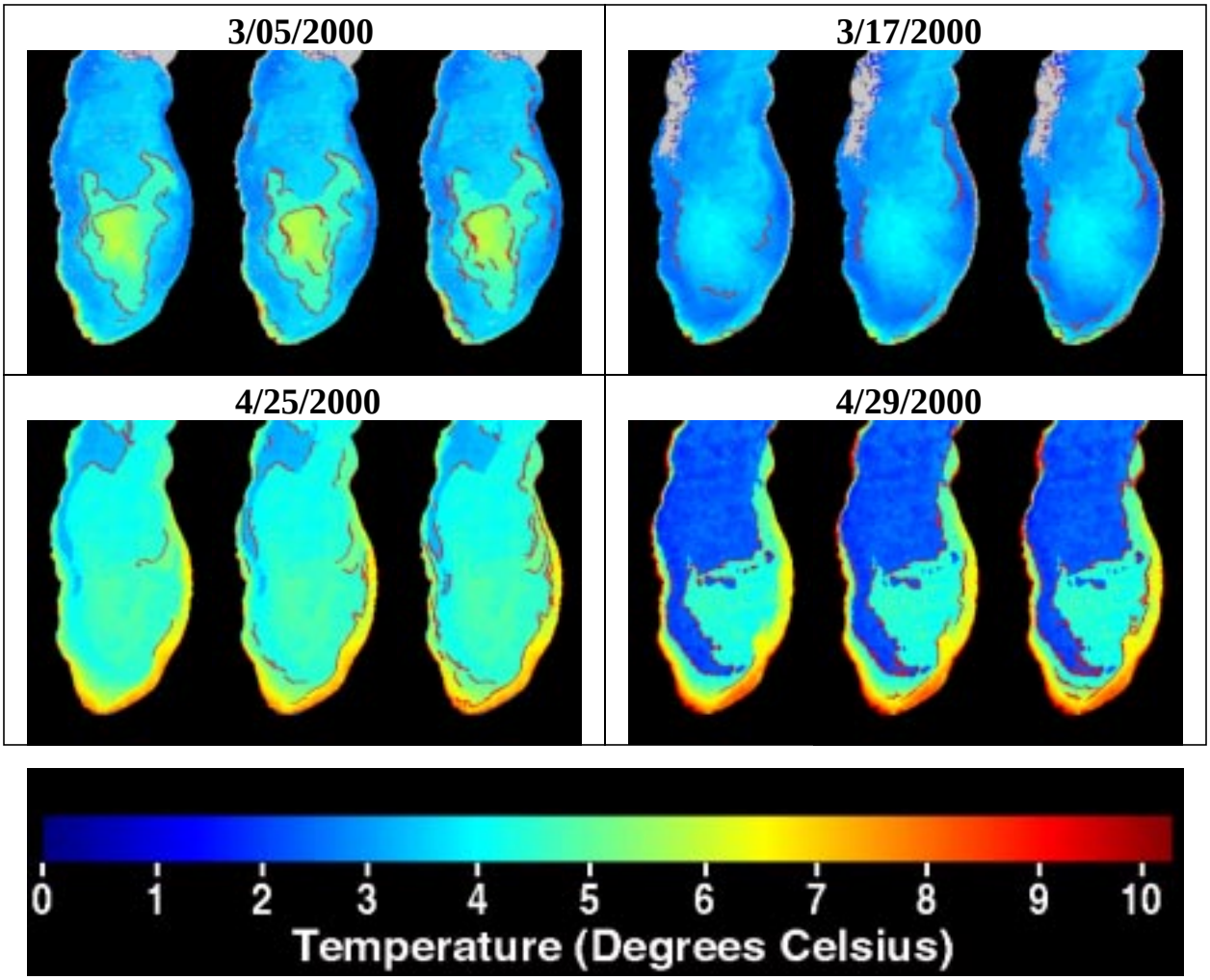

Fig 3- SIED window-level variants run on sea-surface temperature imagery of southern Lake Michigan. Left-most images in each set use the Ullman settings, with a 32x32 pixel window. The middle images use settings found to be optimal for southern Lake Michigan, a 15x15 pixel window. The right images use the VW-SIED algorithm.

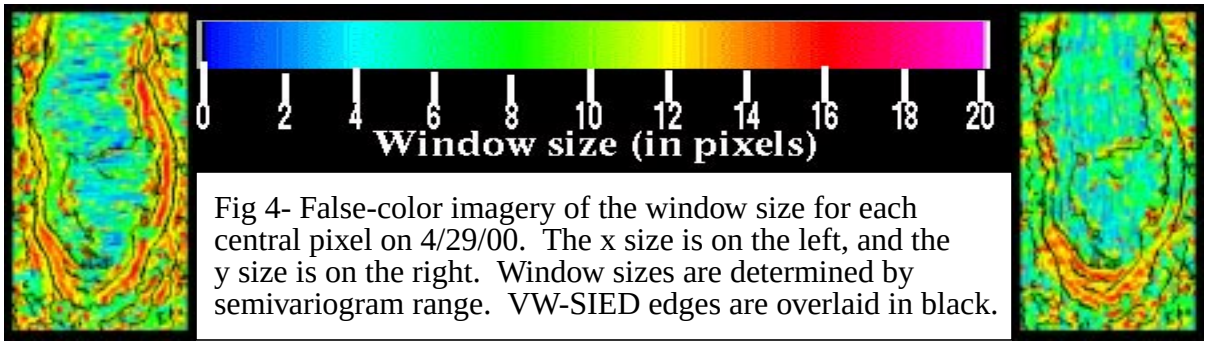

Fig 4- False-color imagery of the window size for each central pixel on 4/29/00. The x size is on the left, and the y size is on the right. Window sizes are determined by semivariogram range. VW-SIED edges are overlaid in black.

HF Radar Observations of Currents, Winds and Waves

John F. Vesecky, P.I., Lorelle A. Meadows, Calvin C. Teague, Pete Hansen, Jeff Paduan, Dan Fernandez and Yolanda Fernandez

Goals

The objective of this portion of the EEGLE research program is to obtain real-time measurements of key air and water variables. These parameters are necessary for the identification and quantification of the physical processes generating cross-margin transport of biologically important material during episodic events. In particular, the HF Radar has been utilized to provide observations of near-surface current and current shear (leading to estimations of wind direction and wave energy) over an area of about 1000 square km adjacent to the Lake Michigan shoreline near St. Joseph/Benton Harbor, Michigan (Fig. 1).

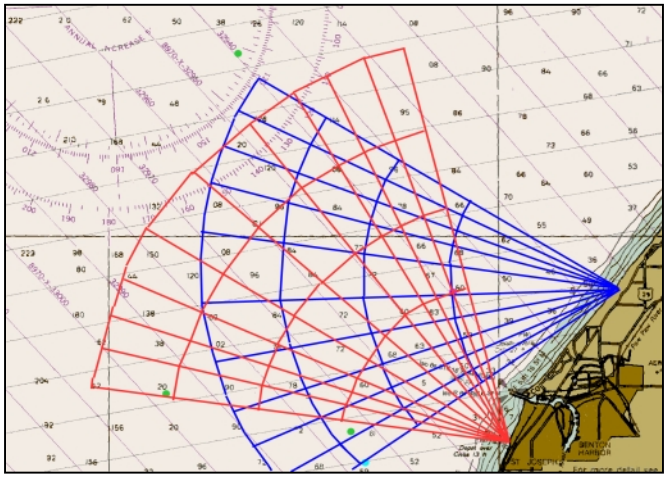

Fig. 1. HF Radar deployment locations and partial antenna patterns

1998 Pilot Experiment

In 1998, the feasibility of utilizing the University of Michigan Multi-frequency Coastal Radar (MCR) units to detect near surface currents over fresh water was tested and proven. This two week pilot deployment, during low energetic wind and wave conditions showed the capability of the radar to detect near-surface current and current shear consistent with ADCP measurements and wind forcing conditions (Vesecky, et al, 1999; Fernandez, et al, 2000).

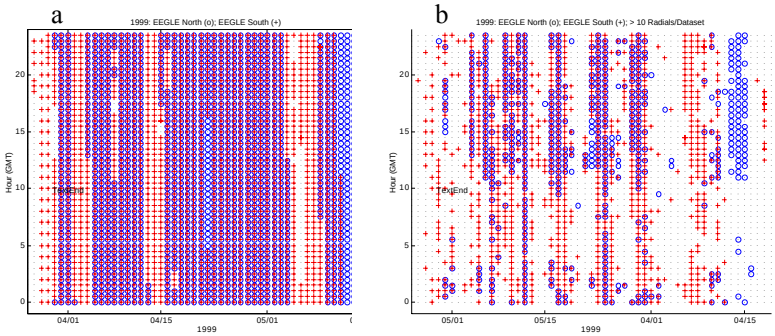

Fig. 2. 1999 HF Radar data sets (a) and data return (b)

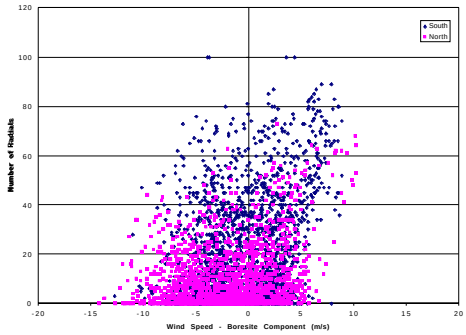

Fig. 3. 1999 data return vs radial wind component

1999 Deployment

In 1999 two MCR units were simultaneously deployed near St. Joseph, Michigan with observational ranges designed to encompass several moored current meters and other in-situ instrumentation (27 March through 18 May). In addition, an Aanderaa Coastal Monitoring (UM Met) buoy was also deployed to measure surface and atmospheric environmental characteristics (25 February through 15 June). This suite of instrumentation provided a coherent package with which to observe changes in environmental parameters and surface dynamic characteristics during the early spring. In particular, the HF Radars were capable of obtaining near surface current and current shear measurements during small episodic sediment suspensions events as well as the progression of the vernal thermal front (Meadows, et al, 2000). Due to the wave conditions during this time period, the northern site had data return of only 32%, further limiting vector current recovery to 20% (Fig. 2 and 3). Despite the small data set, good comparisons were made with ADCP near-surface current measurement (Teague, et al, 2000).

2000 Deployment

Hardware enhancements of the MCR's were completed for the 2000 deployment (1 March to 15 April). Preliminary data analysis reveals stronger return signals at both sites. In addition, stronger onshore wind components during the deployment time (Fig. 4), suggest an improved data return and vector current recovery of 60% for the 2000 deployment.

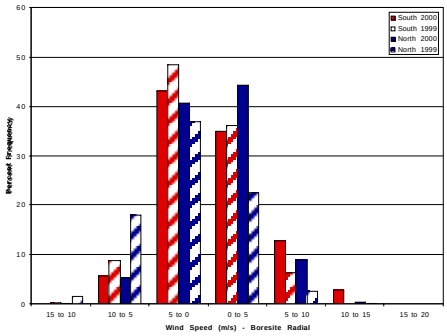

Fig. 4. 1999 vs. 2000 radial wind climate

IEEE Conference on Current Measurement Technology Proceedings, March, 1999.

Surface Current Measurements by HF Radar over Fresh Water at Lake Michigan and Lake Tahoe

John F. Vesecky, Lorelle A. Meadows, Jason M. Daida, Peter E. Hansen, Calvin C. Teague, Daniel M. Fernandez, Jeffrey D. Paduan

HF radar is widely used over salt water to measure surface currents, winds and waves. We report results over fresh water in Lakes Michigan and Tahoe. Although these pilot experiments were brief, they established that useful HF radar observations of surface currents can be obtained out to ranges of about 10 to 15 km with wave heights corresponding to wind speeds of about 3 to 7 m/s. Ranges 2 to 3 times larger and often more would be expected over salt water due to improved ground wave propagation. The currents measured by HF radar closely tracked in-situ current measurements by an acoustic Doppler current profiler. These encouraging results demonstrate the utility of HF radar in freshwater applications, but with significantly less spatial coverage than over salt water.

IEEE Journal of Oceanic Engineering, in press, 2000.

Surface Current Measurements by HF Radar in Fresh Water Lakes

Daniel M. Fernandez, Lorelle A. Meadows, John F. Vesecky, Calvin C. Teague, Jeffrey D. Paduan and Peter Hansen

HF radar has become an increasingly important tool for mapping surface currents in the coastal ocean. However, the limited range, due to much higher propagation loss and smaller wave heights (relative to the salt-water ocean), has discouraged HF radar use over fresh water. Nevertheless, the potential usefulness of HF radar in measuring circulation patterns in fresh water lakes has stimulated pilot experiments to explore HF radar capabilities over fresh water. The Episodic Events Great Lakes Experiment (EEGLE), studying the impact of intermittent strong wind events on the resuspension of pollutants from lake bottom sediments, provided an excellent venue for a pilot experiment. A Multifrequency Coastal HF Radar (MCR) was deployed for 10 days at two sites on the shore of Lake Michigan near St. Joseph, Michigan. Similarly, a single -frequency CODAR SeaSonde instrument was deployed on the California shore of Lake Tahoe. These two experiments showed that when sufficiently strong surface winds ($\geq$ about 7 m/s) exist for an hour or more, a single HF radar can be effective in measuring the radial component of surface currents out to ranges of 10 to 15 km. We also show the effectiveness of using HF radar in concert with acoustic Doppler current profilers (ADCPs) for measuring a radial component of the current profile to depths as shallow as 50 cm and thus potentially extending the vertical coverage of an ADCP array.

IEEE-IGARSS Proceedings, July, 2000.

Multi-Frequency HF Radar Observations of the Thermal Front in the Great Lakes

Lorelle A. Meadows, John F. Vesecky, Calvin C. Teague, Yolanda Fernandez, and Guy A. Meadows

In large fresh water lakes in temperate regions, the spring transition from weak to strong stratification is characterized by the formation of a coastal thermal front. This transition is dominated by high gradients in temperature, nutrient and plankton fields. A combination of solar warming, boundary heat flux, coastal bathymetry and surface wind stress causes the frontal system to develop such that a surface convergence forms at the nearly vertical 4°C isotherm (the temperature of maximum density). This isotherm propagates offshore as warming of the nearshore water increases and as storms provide a mechanism by which the two water bodies (warm stratified nearshore waters and cold isothermal offshore waters) mix. As part of the NSF Episodic Events • Great Lakes Experiment (EEGLE), HF Radar observations were obtained during the development and progression of the vernal thermal bar in Southern Lake Michigan in April 1999. Two Multi-Frequency Coastal Radars (MCR's) were utilized to provide observations of near-surface current vectors and vertical current shear adjacent to the Lake Michigan shoreline near St. Joseph, Michigan. MCR measurements of near-surface currents show evidence of theoretical vernal thermal front circulation supported by in-situ measurements of thermal and dynamic structure. A two-week study of surface dynamics in the vicinity of the thermal front is presented and compared with in-situ measurements.

IEEE-IGARSS Proceedings, July, 2000.

HF Radar Observations of Surface Currents on Lake Michigan During EEGLE 1999

Calvin C. Teague, Lorelle A. Meadows, John F. Vesecky and Yolanda Fernandez

The University of Michigan Multifrequency Coastal Radar (MCR) was used as part of the 1999 Episodic Events Great Lakes Experiment (EEGLE) to measure surface currents on Lake Michigan near St. Joseph, Michigan. High surface-wave loss over fresh water and generally calm wind and wave conditions during the 8-week experiment limited the radar range to less than 10 km. The radar measurements which were obtained showed good agreement (to within about 5 cm s^{-1}) with nearby acoustic Doppler current profiler (ADCP) current meter measurements at 2 m depth. Measurements from the MCR, ADCP and a wind buoy are compared.

The Impact of Episodic Events on Nearshore-offshore Transport in the Great Lakes: Physical Oceanography

P.I.s: J.H. Saylor, G.S. Miller, and M. J. McCormick
Canadian Colleagues: C.R. Murthy, R. Rao, K. Miners, F. Chiocchio, and J. Bull

Objectives

- To identify and quantify the physical processes generating nearshore- offshore transport of biogeochemically important materials during winter/spring episodic events;
- To establish an observation strategy for generating maximum resolution of all the dominant time and space scales;
- To estimate the velocity field along and across the plume as it evolves;
- To determine the coastal energetics of the two-gyre vorticity wave under barotropic conditions and its response to increasing baroclinicity;
- To determine the climatology of coastal energetics of the episodic nearshore current reversals during winter/spring and summer conditions;
- To estimate particle dispersion from Lagrangian statistics and compare with circulation model based estimates to assess model adequacy;
- To undertake a comparative study of coastal ocean processes from this program and past programs undertaken in the Great Lakes;
- To establish a database of all of our observations and make them easily available to other program participants.

Approach

Our observation program is concentrated along the southeast coast of Lake Michigan which, based upon satellite AVHRR data, appears to be the best location for observing cross-margin transport. The observation strategy is based upon moored instrument arrays and Lagrangian measurement.

Results

During the pilot year it was quickly realized that additional data coverage was necessary to augment the observational program. Consequently, GLERL funded scientists from CCIW to participate in EEGLE. In addition to their expertise they brought additional equipment, some of which they deployed in shallow, high risk areas in the primary study region. To date the major focus has been on obtaining and cataloging data from these experiments. Data results are summarized in the following table and some preliminary findings can be found under the products listed on the next page.

Year	Days of temperature data	Days of VACM data	Days of ADCP data	Days of SACM data	Days of drifter data
'97-'98	11,940	4,030	890	-	55
'98-'99	29,785	7,020	2,020	1,540	400
'99-'00	18,515	5,400	1,560	1,450	310

Products

Publications:

Miller, G. S., Saylor, J. H. and M. J. McCormick. 1999. Detecting storm-generated suspended materials in Lake Michigan using ADCP echo intensities. Proceedings of IEEE Sixth Working Conference on Current Measurement. San Diego, CA.

McCormick, M. J., and G. L. Fahnenstiel. 1999. Recent climatic trends in nearshore water temperatures in the St. Lawrence Great Lakes. **Limnol. and Oceanog.** 44(3):530-540.

Beletsky, D., Schwab, D. J., McCormick, M. J., Miller, G. S., Saylor, J. H., and P. J. Roebber. 2000. Hydrodynamic modeling for the 1998 Lake Michigan coastal turbidity plume event. Proceedings of the 6th International Conference on Estuarine and Coastal Modeling (In Press).

Helfand, J. S., Podber, D. P., and M. J. McCormick. 2000. Effect of heat flux on thermocline formation. Proceedings of the 6th International Conference on Estuarine and Coastal Modeling (In Press).

Presentations:

McCormick, M. J., Miller, G. S., Murthy, C. R., and J. H. Saylor. 2000. Observations of the coastal flow in southern Lake Michigan. Ocean Sciences Meeting. AGU-ASLO, Jan. 24-28. San Antonio, TX

Saylor, J. H., McCormick, M. J., Miller, G. S., and C. R. Murthy. 1999. Observations of cross-shelf currents and sediment transport in the coastal boundary layer of southeastern Lake Michigan. AGU Fall Meeting. Dec. 13-17. San Francisco, CA.

Beletsky,D., D.J. Schwab, M.J. McCormick, G. S. Miller, J.H. Saylor, and P.J. Roebber. 1999. Hydrodynamic modeling for the 1998 Lake Michigan coastal turbidity plume event. The 6th International Conference on Estuarine and Coastal Modeling, November 3-5, 1999, New Orleans, LA.

Helfand, J. S., Podber, D. P., and M. J. McCormick. 1999. Effect of heat flux on thermocline formation. The 6th International Conference on Estuarine and Coastal Modeling. November 3-5, 1999. New Orleans, LA.

Saylor, J. H., Miller, G. S., and M. J. McCormick. 1999. Observations of sediment resuspension and transport in the coastal and bottom boundary layers of large lakes with Acoustic Doppler Current Profilers. IUGG XXII Conference. July 19-30. Birmingham, UK.

Saylor, J. H., Miller, G. S., and M. J. McCormick. 1999. Measurements of sediment resuspension and transport in Lakes Michigan and Champlain using Acoustic Doppler Current Profilers. Conference on the Adirondacks and the Lake Champlain Basin, Lake Saranac, New York, May 26-28.

McCormick, M. J., Murthy, C. R., Miller, G. S., and J. H. Saylor. 1999. Measuring offshore and longshore transport with current meter arrays during storm events in Lake Michigan. Amer. Soc. Limnol. Oceanogr. Feb. 1-5. Sante Fe, NM.

The Impact of Episodic Events on Nearshore-offshore Transport in the Great Lakes: Hydrodynamic Modeling Program

PI's: David J. Schwab and Dmitry Beletsky

Objectives:
The main objective of this proposal is to identify and quantify the physical processes generating nearshore- offshore transport of biogeochemically important materials in the Great Lakes during episodic events by applying a coupled ice-circulation model to Lake Michigan. The specific objectives include:

- To determine the role of ice in timing and magnitude of the plume events
- To determine whether the plume occurrence represents a response to the aggregate effects of a season of individual storm events, an episodic response to a single large storm event or a complex interaction between the low-frequency (seasonal) preconditioning of the lake and a single storm event that occurs at a critical time.
- To determine the importance of mesoscale atmospheric dynamics on the development of the plume.
- To determine the role of local bathymetry in the separation/meandering of the plume.
- To determine the influence of thermal effects on the dynamics of the plume.
- To refine the ice and circulation models using the results of an extensive observation program.
- To link the ice-circulation model and the Lake Michigan wind wave prediction model with a sediment resuspension/transport model in order to quantify the cross-isobath transport of resuspended material in the lake.
- To link the ice-circulation model with a nutrient and lower food web model in order to investigate the impact of nearshore-offshore transport during episodic events on biological processes in the lake.
- To incorporate the results of these investigations into a computer-based Information and Forecasting System.

Approach:

1. Ice Modeling – develop Great Lakes Ice Model
2. Circulation Modeling – apply Great Lakes version of Princeton Ocean Model to Lake Michigan for EEGLE study years
3. Wave Modeling - apply GLERL/Donelan Wave Model to Lake Michigan for EEGLE study years
4. Integration with Sediment Transport Modeling and Lower Food Web Modeling Projects

Results:

1. The spectacular eddy-like plume that occurred during the 1998 EEGLE pilot year was used as a case study for coupled hydrodynamic/wave/sediment transport and coupled hydrodynamic/biological models. The case studies confirmed the episodic nature of lake circulation and sediment transport in the lake as well as identifying light limitation from suspended material in the plume region as a critical factor in primary production.
2. The combination of high waves and the two-gyre circulation pattern in southern Lake Michigan during storms with northerly winds appears to be responsible for the asymmetric distribution of bottom sediments in the lake.
3. During the unusually warm EEGLE pilot year and field years the role of ice in plume formation was a negligible factor so the work on developing a Great Lakes ice model was postponed.

Collaborators: Roebber, Saylor et al., Vesecky, Budd et al., Bedford et al., Chen

Estuarine, Coastal and Shelf Science (2000) **50,** 49–58
Article No. ecss.1999.0531, available online at http://www.idealibrary.com on IDEAL®

The 1998 Coastal Turbidity Plume in Lake Michigan

D. J. Schwab[a,c], D. Beletsky[b] and J. Lou[a]

[a]*NOAA Great Lakes Environmental Research Laboratory, 2205 Commonwealth Blvd., Ann Arbor, MI 48105, U.S.A.*
[b]*Department of Naval Architecture and Marine Engineering, University of Michigan; Cooperative Institute for Limnology and Ecosystems Research/NOAA Great Lakes Environmental Research Laboratory and University of Michigan, Ann Arbor, MI 48105, U.S.A.*

Received 17 November 1998 and accepted in revised form 22 March 1999

In this paper, numerical models of coastal circulation, wind-waves, and sediment transport are applied to the March 1998 turbidity plume event in Lake Michigan to investigate the role of wind-induced circulation in the offshore transport of sedimentary material in Lake Michigan. Computer visualization is used to compare model results to the evidence of cross-isobath transport suggested in satellite imagery. Model results showed that circulation in Lake Michigan is highly episodic since it is almost entirely wind-driven in early spring. The characteristic wind-driven circulation pattern in the lake consists of two counter-rotating gyres, a counterclockwise-rotating gyre to the right of the wind, and a clockwise-rotating gyre to the left. The gyres are separated by a convergence zone along the downwind shore with resulting offshore flow and a divergence zone along the upwind shore with onshore flow. This two-gyre circulation pattern with offshore flow was very clearly seen during a northerly wind event in March 1998 in southern Lake Michigan. The strongest sediment resuspension occurred in the southern lake and the shallow waters along the coastline. This is because of the larger waves in southern Lake Michigan due to the dominant northerly wind in this early spring period. The two most significant sediment resuspension events were detected in the model results during the two storm events. Although results from the sediment transport model agree qualitatively with satellite imagery, they fail to simulate the initial eddy-like structure of the plume. Visualization is shown to be an effective tool for interpreting the complex turbidity patterns in the satellite imagery of the turbidity plume.

Keywords: sediment transport; numerical model; coastal currents; wind waves; visualization

Introduction

In the North American Great Lakes, as well as in the coastal ocean, the gradients of many biogeochemically important materials (BIMs) are considerably higher in the offshore direction than in the longshore direction (Brink *et al.*, 1992; Scavia & Bennett, 1980). In the presence of these large gradients, cross-isobath circulation is a primary mechanism for the exchange of material between nearshore and offshore waters. Both the alongshore and cross-isobath components of the current exhibit strong episodic behaviour due to wind forcing. As opposed to alongshore transport, the advective and diffusive mechanisms driving cross-isobath transport and the time scales over which they operate have not been extensively studied. A necessary step in understanding cross-isobath transport of BIMs is to identify and quantify the physical processes that are responsible for the nearshore-offshore water mass and material exchange. To this end, a multidisciplinary research program jointly sponsored by NOAA (National Oceanic and Atmospheric Administration) and NSF (National Science Foundation) was recently initiated to study the recurrent turbidity plume in southern Lake Michigan (http://www.glerl.noaa.gov/eegle).

In the context of nearshore–offshore transport, the Great Lakes present somewhat different challenges than the continental shelf. Although many of the physical processes responsible for the movement of material from the coastline toward deeper waters are similar in both environments, the fact that the lakes are fully enclosed by land has significant consequences. When material is transported offshore in the Great Lakes, it can only be removed from the system by permanent burial in the sediments or removal through an outflow. This is in contrast to the continental shelf where transport across the shelf break to the deep ocean can also be considered a removal mechanism. The physical mechanisms for cross-shelf transport are

Full sized figures, tables and animations are stored on the CD-ROM accompanying this article. Use a Web browser to access the start page ‘default.htm’ and follow the links. The help file ‘help.htm’ provides answers for some common problems.

[c]E-mail: schwab@zeus.glerl.noaa.gov

0272–7714/00/010049+10 $35.00/0

similar, and in some cases identical, to the processes that control nearshore-offshore transport in the lakes, but there is no analogue in the lakes for exchange with the deep ocean across the shelf break.

Recent satellite observations of suspended sedimentary material in Lake Michigan (Eadie *et al.*, 1996) offer a unique opportunity to investigate a recurrent episode of cross-isobath transport. A 10 km wide plume of resuspended material extending over 100 km along the southern shore of the lake was first observed in satellite imagery by Mortimer (1988), and has been observed every spring since 1992, when satellite imagery for the Great Lakes region first became available on a routine basis through the NOAA CoastWatch program (Schwab *et al.*, 1992). The bathymetry and geometry of the Lake Michigan basin are shown in Figure 1. The resuspension plume of March 1998 was one of the largest events of record. Satellite observations (Figure 2) reveal a well developed plume extending over 300 km of coastline from Milwaukee, WI (station MKE in Figure 1) to Muskegon, MI (station MKG in Figure 1) with several dominant offshore features originating from the south-eastern shoreline. The plume originated around March 10 following several days of intense storms that produced 17 m s^{-1} northerly winds and generated waves in the basin over 5 m high. Remnants of the plume feature were still observable by satellite six weeks later. Our current understanding is that the initiation of the plume is caused by a major storm with strong northerly winds generating large waves in southern Lake Michigan. The plume appears along the entire southern coastline of the lake. It occasionally veers offshore along the eastern shore of the lake, coincidentally near the areas of highest measured long-term sediment accumulation in the lake (Figure 3). The offshore structure of the turbidity plume often resembles the structure of cold water filaments seen in thermal imagery of the California Current by Strub *et al.* (1991) and others.

Considerable progress has recently been made in developing two and three dimensional circulation models for the Great Lakes. Numerical hydrodynamic models are now able to simulate large scale circulation in the lakes with reasonable accuracy (Schwab & Bedford, 1994; Beletsky *et al.*, 1997). It is possible to resolve kilometre scale variability in current and temperature fields with high resolution versions of these models. In addition, a parametric surface wind wave model developed by Schwab *et al.* (1984) is available for modelling waves at these same scales. This model has been shown to provide excellent estimates of wave height and wave direction for fetch-limited waves in several applications to the Great Lakes (Liu *et al.*, 1984; Schwab & Beletsky, 1998). Furthermore, a quasi-3-D suspended sediment transport model developed by Lou *et al.* (1999) has recently been coupled with the circulation and wind wave models to provide estimates of suspended sediment concentration at similar resolutions. In this paper, we apply the circulation, wind-wave, and sediment transport models to the March 1998 turbidity plume event in Lake Michigan to investigate the role of wind-induced circulation in the offshore transport of sedimentary material in Lake Michigan. Computer visualization is used to compare model results to the evidence of cross-isobath transport suggested in satellite imagery.

Wave model

The wave model is a numerical finite-difference solution to the two-dimensional wave momentum conservation equation. The wave energy spectrum is parameterized at each point on a rectilinear computational grid in terms of total wave energy, peak energy period, and predominant wave direction. The momentum balance equation is

$$\frac{\partial \boldsymbol{M}}{\partial t} + \boldsymbol{v}_g \nabla \boldsymbol{M} = \boldsymbol{\tau}_w$$

where ∇ is the horizontal gradient operator, and $\boldsymbol{M}$ and $\boldsymbol{v}_g$ are the total momentum vector and the corresponding group velocity vector, and $\boldsymbol{\tau}_w$ is that part of the momentum input from the wind that produces net wave momentum growth. The directional wave energy spectrum is assumed to have a cosine-squared angular dependence about a single dominant mean wave direction which is independent of frequency.

Momentum input from the wind consists of two components, one ($\boldsymbol{\tau}_1$) parallel to the wind vector and the other ($\boldsymbol{\tau}_2$) parallel to the wave momentum vector, i.e.

$$\boldsymbol{\tau}_w = \boldsymbol{\tau}_1 + \boldsymbol{\tau}_2$$

The scalar values of the two components as suggested by Donelan (1979) are:

$$\tau_1 = \frac{\gamma}{2} \rho_a D_1 |U - 0{\cdot}83 c_p \cos\theta_0| (U - 0{\cdot}83 c_p \cos\theta_0)$$

$$\tau_2 = \frac{\gamma}{2} \rho_a D_2 |U\cos\theta_0 - 0{\cdot}83 c_p| (U\cos\theta_0 - 0{\cdot}83 c_p)$$

where c_p is the wave phase velocity, ρ_a is the air density, U is the 10 m wind speed, θ_0 is the angle

between the wind and the waves, $\gamma(=0{\cdot}028)$ is the empirical fraction of the wind stress that is retained by the waves, and D_1 and D_2 are form drag coefficients given by

$$D_1=[0{\cdot}4/\ln(50/\xi\cos\theta_0)]^2$$

$$D_2=[0{\cdot}4/\ln(50/\xi)]^2$$

where ξ is the root mean square surface elevation (in metres). Both τ_1 and τ_2 may be positive, indicating wave growth, or negative, indicating wave decay.

To solve the momentum balance equation we use an empirical relationship between wave momentum and wave height derived from JONSWAP relations (Hasselman *et al.*, 1973) linking ξ^2 with peak energy frequency, f_p, and mean wind U:

$$\xi^2=6{\cdot}23\times10^{-6}\left(\frac{f_pU}{g}\right)^{-10/3}\frac{U^4}{g^2}$$

The model is thus semi-empirical and parametric. A simple numerical integration scheme can then be applied to the momentum balance equation. Forward time differences are used to calculate the momentum components at the centre of the grid squares, and a combination of upwind and centred differences are used to evaluate the momentum advection terms at the edges of the grid squares. Model output at each grid point consists of significant wave height (defined by $H_{1/3}=4\xi$), peak-energy wave period and average wave direction.

The model is applied on a 2 km rectilinear grid covering Lake Michigan. Output from the 2 km wave model (wave height and wave period) is used to estimate bottom shear stress in the sediment transport model described below.

Hydrodynamic model

A three-dimensional circulation model for the Great Lakes (Schwab & Beletsky, 1998) is used to calculate lake circulation. The model is based on the Princeton Ocean Model (Blumberg & Mellor, 1987) and is a nonlinear, fully three-dimensional, primitive equation, finite difference model. The model is hydrostatic and Boussinesq so that density variations are neglected except where they are multiplied by gravity in the buoyancy force. The model uses time-dependent wind stress and heat flux forcing at the surface, zero heat flux at the bottom, free-slip lateral boundary conditions, and quadratic bottom friction. The drag coefficient in the bottom friction formulation is spatially variable. It is calculated based on the assumption of a logarithmic bottom boundary layer using a constant bottom roughness of 1 cm.

To simplify the discussion of model physics, we present the dynamical equations in Cartesian co-ordinates. The velocity components (u,v,w) are in the (x,y,z) directions. The mass continuity equation is

$$\nabla\boldsymbol{V}+\frac{\partial w}{\partial z}=0$$

where $\mathbf{V}=(u,v)$ is the horizontal velocity. The horizontal momentum equations are

$$\frac{\partial u}{\partial t}+\boldsymbol{V}\nabla u+w\frac{\partial u}{\partial z}-fv=-\frac{1}{\rho_0}\frac{\partial p}{\partial x}+\frac{\partial}{\partial x}\left(A_M\frac{\partial u}{\partial x}\right)+\frac{\partial}{\partial y}\left(A_M\frac{\partial u}{\partial y}\right)+\frac{\partial}{\partial z}\left(K_M\frac{\partial u}{\partial z}\right)$$

$$\frac{\partial v}{\partial t}+\boldsymbol{V}\nabla v+w\frac{\partial v}{\partial z}+fu=-\frac{1}{\rho_0}\frac{\partial p}{\partial y}+\frac{\partial}{\partial x}\left(A_M\frac{\partial v}{\partial x}\right)+\frac{\partial}{\partial y}\left(A_M\frac{\partial v}{\partial y}\right)+\frac{\partial}{\partial z}\left(K_M\frac{\partial v}{\partial z}\right)$$

where ρ is density, p is pressure, f is the Coriolis parameter, and A_M and K_M are the horizontal and vertical momentum eddy viscosities, respectively. The Eulerian derivatives at a point are the result of the horizontal and vertical velocity advections, horizontal pressure gradient force, Coriolis force, and horizontal and vertical momentum diffusion. Horizontal diffusion is calculated with a Smagorinsky eddy parameterization (with a multiplier of 0·1) to give a greater mixing coefficient near strong horizontal gradients.

The Princeton Ocean Model employs a terrain following vertical co-ordinate system (σ- co-ordinate) which replaces the vertical co-ordinate, z, with a normalized vertical co-ordinate, $\sigma=(z-\eta)/(d+\eta)$, where d is the local depth, and η is the free surface elevation. The advantage of this system is that in the transformed co-ordinate system, the bottom corresponds to a uniform value of the vertical co-ordinate ($\sigma=-1$), thus simplifying the governing transport and continuity equations. The hydrodynamic model of Lake Michigan has 20 vertical levels and a uniform horizontal grid size of 2 km.

The equations are written in flux form, and the finite differencing is done on an Arakawa-C grid using a control volume formalism. The finite differencing scheme is second order and centred in space and time (leapfrog). The model includes the Mellor and Yamada (1982) level 2·5 turbulence closure parameterization for calculating the vertical mixing

coefficients for momentum K_M, and heat, K_H, from the variables describing the flow regime.

The output from the lake circulation model is used to provide estimates of horizontal advection and bottom shear stress for the sediment resuspension and transport model. In addition, the turbulence closure scheme in the circulation model can provide estimates of physical dispersion coefficients for water quality and toxics models.

Suspended sediment transport model

The suspended sediment transport model is a quasi-3-D model based on an asymptotic solution for uniform flow to the convection-diffusion equation as described by Galappatti and Vreugdenhil (1985). In the present model, this approach has been developed into more complicated flow fields and generalized to the combined wave-current situations.

The suspended particles are assumed to be so small that their motions relative to ambient fluid fall into Stokes' range. The basic equation describing mass conservation of suspended sediment in a turbulent flow can be expressed as:

$$\frac{\partial c}{\partial t}+u\frac{\partial c}{\partial x}+v\frac{\partial c}{\partial y}+(w-w_s)\frac{\partial c}{\partial z}=\frac{\partial}{\partial x}\left(\varepsilon_x\frac{\partial c}{\partial x}\right)+\frac{\partial}{\partial y}\left(\varepsilon_y\frac{\partial c}{\partial y}\right)+\frac{\partial}{\partial z}\left(\varepsilon_z\frac{\partial c}{\partial z}\right)$$

where ε_x, ε_y, ε_z are sediment particle diffusion coefficients in the x, y, z directions for the combined motion of waves and currents, and $c(x,y,z,t)$ is the suspended sediment concentration.

The wave effect is taken into account by assuming an analogy of mixing profile on a wave-averaged and turbulence-averaged scale and the modified eddy viscosity coefficient (Van Rijn, 1985), as well as by introducing an enhanced bottom shear stress (Lou & Ridd, 1996). In cases where suspended load is the main mode of sediment transport, an asymptotic solution of the convection-diffusion equation is presented. The vertical concentration structure has been shown to depend only on the vertical velocity profile and the mixing coefficient, and thus can be calculated in advance (Lou, 1995). As a result, the three-dimensional concentration problem is separated into two parts: a two-dimensional depth-averaged sediment concentration model and vertical concentration profiles being solved in advance.

The bottom shear stresses required by the sediment transport model for bottom boundary condition were calculated by a bottom boundary layer model. The effect of nonlinear wave-current interaction on the bottom shear stress was obtained based on the concept of Grant and Madsen (1979) in an iterative form (Lou & Ridd, 1997).

A three layer wave-induced diffusion coefficient (Van Rijn, 1986) was proposed in the sediment concentration model. The sediment mixing coefficient due to the combination of waves and current is assumed to be given by the sum of the squares of the current-related ($\varepsilon_{s,c}$) and wave-related ($\varepsilon_{s,w}$) values:

$$\varepsilon_s^2=\varepsilon_{s,c}^2+\varepsilon_{s,w}^2$$

The current-related turbulent eddy coefficient $\varepsilon_{s,c}$ is calculated numerically from the 3-D circulation model.

The bottom boundary conditions in the sediment transport model were evaluated at a reference water-sediment interface level $z=a$. The upward flux of suspended sediment at this reference level can be given by:

$$F_a=w_s(E_s-c_a\cos\theta)$$

where, c_a is the near bed concentration of suspended sediment, $w_s c_a \cos\theta$ is the deposition rate per unit bed area due to the fall velocity w_s, θ is the bottom slope and E_s is a dimensionless coefficient describing the entrainment of bottom sediment into suspension due to turbulence.

A similar entrainment coefficient described by Garcia and Parker (1991) was adopted in our study as follows:

$$E_s=\frac{AZ_k^5}{1+\frac{A}{0{\cdot}3}Z_k^5}$$

where

$$Z_k=\frac{u'_\star}{w_s}\left[\frac{\sqrt{(s-1)gD_k}}{v}D_k\right]^{0{\cdot}6}$$

A is a constant ($=1{\cdot}3\times10^{-7}$), s is the specific density, $u'_\star$ is the bottom shear velocity, D_k is the characteristic size of sediment, and v is the kinetic viscosity.

The suspended sediment concentration at reference level $z=a$ above the bed is expressed as (Van Rijn, 1989):

$$c_a=0{\cdot}015\frac{D_{50}}{a}\frac{T^{1{\cdot}5}}{D_\star^{0{\cdot}3}}$$

where

$$T=\frac{(\tau_b-\tau_{b,cr})}{\tau_{b,cr}}$$

τ_b is the effective bed shear stress under combined waves and current, and $\tau_{b,cr}$ the time-averaged Shields critical shear stress.

To reduce numerical dispersion, the second order upwind difference scheme has been applied to the horizontal advection terms. A hybrid Crank-Nicolson and ADI solution scheme is developed to calculate the concentration results. In the model application to Lake Michigan, a uniform 2 km horizontal grid mesh, 20 vertical layers, and a staggered C-grid arrangement were employed for the sediment transport model, which are compatible with the circulation and wind wave models mentioned above.

Forcing functions

To calculate momentum flux fields over the water surface for the lake circulation and wave models, it is necessary to estimate wind and air temperature fields at model grid points. Meteorological data were obtained from 12 National Weather Service stations around Lake Michigan (Figure 1). These observations form the basis for generating gridded overwater wind and air temperature fields.

Overland wind speeds generally underestimate overwater values because of the marked transition from high aerodynamic roughness over land to much lower aerodynamic roughness over water. This transition can be very abrupt so that wind speeds reported at coastal stations are often not representative of conditions only a few kilometres offshore. Schwab and Morton (1984) found that wind speeds from overland stations could be adjusted by empirical methods to obtain fair agreement with overlake wind speeds measured from an array of meteorological buoys in Lake Erie. For meteorological stations that are more representative of overland than overwater conditions, namely all stations except SGNW3 in Figure 1, the empirical overland-overlake wind speed adjustment from Resio and Vincent (1977) is applied.

To interpolate meteorological data observed at irregular points in time and space to a regular grid so that it can be used for input into numerical wave, sediment transport, and circulation models, some type of objective analysis technique must be used. For this study the nearest-neighbour technique was used, with the addition of a spatial smoothing step (with a specified smoothing radius). In the nearest neighbour technique, observations from up to three hours before the interpolation time to three hours after the interpolation time are also considered. In the nearest-neighbour distance calculations, the distance from a grid point to these observation points is increased by the product of the time difference multiplied by a scaling speed. The interpolation scaling speed is taken as $10\ \mathrm{km\ h^{-1}}$. Interpolation smoothing distance is 30 km. It was found that the nearest-neighbour technique provided results comparable to results from the inverse power law or negative exponential weighing functions discussed in Schwab (1989).

Results

Hourly meteorological data from the 12 stations shown in Figure 1 were obtained for the period 1–30 March, 1998. Overwater wind and air temperature fields were interpolated to the 2 km grid. Time series of wind speed and direction from a point in the middle of the southern basin (Figure 1) are shown in Figure 4. There are four major wind events in March, two storms with northerly winds (on the 9th and 21st) and two with southerly winds (on the 13th and 27th). In early spring, the lake is thermally homogeneous and density gradients are negligible. Therefore, the circulation model was applied in a barotropic mode with uniform (2 °C) water temperature. The wave model was used to compute hourly values of wave height, wave period, and wave direction, from which wave-induced bottom orbital velocity was calculated. The evolution of the computed wave height field for the 30 day simulation period is illustrated in Animation 1. Time series of wave model results for wave height, period, and direction at a point in the middle of the southern basin (Figure 1) are presented in Figure 4. The largest wave heights in the southern basin occur during the storms with northerly winds which provide the longest overwater fetch distance. The circulation model computed hourly values of horizontal currents and dispersion coefficients. The suspended sediment transport model then was used to simulate suspended sediment concentration during this period.

The computed circulation is illustrated through the use of a computer animation in Animation 2. The animation depicts the trajectories of passive tracer particles which were introduced into the computed depth-averaged velocity field on 1 March and are traced through the 30 day computational period. The mean wind vector is also shown. Particle trajectories are computed using the technique developed by Bennett *et al.* (1983) and Bennett and Clites (1987). This technique includes a method for interpolating the computed velocity field from velocity points on the computational grid to the particle locations, which minimizes collisions of the particles with the shoreline. Particles are initially located in the centre of every third grid cell. In order to more clearly illustrate the effect of lake circulation on cross-isobath transport,

particles initially placed in cells with depth less than 30 m are coloured orange in the animation.

In the animation a new visual technique is used to enhance the perception of fluid motion. Particle locations at each time step are depicted by a bright spot. Previous locations of that particle for the last 48 h are also depicted as spots of diminishing intensity. The visual effect is that of a ' tail ' on each particle whose length indicates the particle's speed and whose position indicates a history of the particle's recent locations. This technique is also useful for producing a ' snapshot ' of currents at a single time which also gives an indication of current magnitude and direction over the previous 48 h.

The time evolution of the modelled surface suspended sediment concentration in Lake Michigan is depicted in Animation 3. The model started from zero concentration over the whole lake as the initial condition on 1 March 1998. The dominant sediment particle size is assumed to be 15 μm, the settling velocity is set to 0·5 m day^{-1}, the critical bottom shear stress is 0·05 Nm^{-2}, and the bottom of the lake is treated as an unlimited sediment source. The animation shows colour contour maps of surface suspended sediment concentration at 3 h intervals. It illustrates the hydrodynamic effects on sediment resuspension and transport resulting from the interactions among sediment, topography, circulation and wind waves in Lake Michigan.

A simple estimation of sediment erosion and deposition is made based on the sediment transport results in March 1998, with the purpose of highlighting the hydrodynamic effects on sediment redistribution in the lake. During the course of model simulation, the sediment layer thickness changes with sediment erosion from the bottom or deposition from the water column. The erosion and deposition areas were determined by comparing the final sediment layer thickness with the initial thickness. The net change in bed thickness resulting from the March 1998 simulation is given in Figure 7.

Discussion

Model results showed that circulation in Lake Michigan is highly episodic since it is almost entirely wind-driven in early spring. The characteristic wind-driven circulation pattern in a lake consists of two counter-rotating gyres: a counterclockwise-rotating (cyclonic) gyre to the right of the wind and a clockwise-rotating (anticyclonic) gyre to the left (Bennett, 1974). The gyres are separated by a convergence zone along the downwind shore with resulting offshore flow and a divergence zone along the upwind shore with onshore flow. This two-gyre circulation pattern was very clearly seen during several wind events in March in southern Lake Michigan (Animation 2 and Figure 5). The first storm with northerly winds up to 17 m s^{-1} on 9 March caused strong along-shore southerly currents that converged near Benton Harbor, Michigan (station BEH in Figure 1) and caused massive offshore flow lasting several days. The second northerly storm on 21 March also produced a two-gyre circulation pattern in southern Lake Michigan, but with a cyclonic gyre which was more prominent than the anticyclonic gyre. Finally, southerly winds on 26–27 March created a ' reversed ' two-gyre circulation pattern with onshore flow near Benton Harbor instead of offshore flow. We were not able to reproduce the spectacular spiral eddy observed in the middle of the lake on 12 March (Figure 2) which is probably a result of meandering of the strong offshore jet.

Sediment concentration results showed that at least some suspended sediment was present during most days of March 1998 (Figure 6 and Animation 3). The strongest sediment resuspension mainly occurred in the southern lake and the shallow waters near the coastline. This is caused by the larger waves in southern Lake Michigan due to the dominant northerly wind in this early spring period. The two most significant sediment resuspension events were detected in the model results on 9–12 March and 20–22 March, which coincide with the strongest northerly winds as shown in Figure 4.

The first storm caused strong sediment resuspension (with concentration values above 10 mg l^{-1}) in coastal areas within the 30 m isobath after 8 March (Animation 3). Large waves (over 5 m) were responsible for the local resuspension along the coastline and mid-lake ridge area, and the strong currents determined the plume advection. The most significant activity occurred along the southern and south-eastern shoreline during 10–12 March and 21–23 March. The sediment model was not able to simulate the observed offshore spiral eddy structure on 12 March. The second resuspension event also occurred under northerly wind conditions on 21 March. The sediment concentration results showed a similar pattern but with somewhat smaller magnitudes. Another noticeable phenomenon in the model results is evidence of high offshore suspended sediment concentration near the south-eastern corner of the lake during the 9–12 March storm, and a similar pattern after 21 March. From the circulation model results (Figure 5 and Animation 2), it is clearly seen that this high offshore sediment concentration coincided with strong offshore flow, which may have moved the

material from the coastal area to the deeper waters. Similar offshore sediment transport was also seen in previous plume events, with the offshore flow occurring at slightly different sites along the south-eastern shoreline depending on wind direction. Since the area of high offshore sediment concentration also coincides with an area of strong currents, the high sediment concentration in the model may also be caused by local resuspension rather than advection or diffusion.

As shown in Figure 7, net erosion during the storm events in March 1998, occurred mainly along the shoreline and deposition occurred offshore. Overall, the deposition pattern during this event is similar to the long term sediment accumulation map shown in Figure 3. Both show an asymmetric pattern of sediment deposition, with maximum deposition occurring mainly in the eastern side of the lake in water depths of 50–100 m. This asymmetric pattern was basically established after the first wind event and did not change much during the rest of the month, which tends to support the hypothesis that the long term sediment deposition pattern may be largely determined by a few major storm events. The largest net deposition occurred in the southern and south-eastern part of the lake and around the mid-lake ridge area. The net sediment accumulation in the southern lake is consistent with the circulation convergence zone and its extension offshore, where the sediment particles suspended by the high erosion along the western and eastern shores were probably transported by the large offshore currents. The greatest erosion occurred along the western shore and also in the mid-lake ridge area. Given that the bottom sediment dry bulk density is 1450 kg m^{-3}, the estimated total resuspended sediment mass in March 1998 in Lake Michigan was $7{\cdot}53 \times 10^9$ kg.

Though the sediment transport model can depict the resuspension events reasonably well, it was not able to describe the detailed plume structure, particularly the spiral eddy in the central part of southern lake. Because the offshore structure of the sediment plume depends strongly on the circulation patterns, we believe that inaccuracies in the hydrodynamic model results could well be responsible for the missing features. To study this unique process further, more hydrodynamic and sediment transport studies are needed in the future. More experiments are underway to study effects of wind field interpolation, grid resolution, and friction on hydrodynamics and sediment dynamics in Lake Michigan.

Acknowledgements

This is GLERL Contribution No. 1124. This work is part of the EEGLE (Episodic Events—Great Lakes Experiment) Program sponsored by the National Science Foundation and the National Oceanic and Atmospheric Administration Coastal Ocean Program. J.L. was supported by the National Research Council's Research Associateship Program.

References

Beletsky, D., O'Connor, W. P., Schwab, D. J. & Dietrich, D. E. 1997 Numerical simulation of internal Kelvin waves and coastal upwelling fronts. *Journal of Physical Oceanography* **27,** 1197–1215.

Bennett, J. R. 1974 On the dynamics of wind-driven lake currents. *Journal of Physical Oceanography* **4,** 400–414.

Bennett, J. R., Clites, A. H. & Schwab, D. J. 1983 A two-dimensional lake circulation modeling system: programs to compute particle trajectories and the motion of dissolved substances. *NOAA Tech. Memo. ERL GLERL-46*. NOAA Great Lakes Env. Res. Lab., Ann Arbor, MI, 51 pp.

Bennett, J. R. & Clites, A. H. 1987 Accuracy of trajectory calculation in a finite-difference circulation model. *Journal of Computational Physics* **68,** 272–282.

Blumberg, A. F. & Mellor, G. L. 1987 A description of a three-dimensional coastal ocean circulation model. In *Three dimensional Coastal Ocean Models, Coastal and Estuarine Sciences* 5 (Heaps, N. S., ed.), American Geophysical Union, Washington D.C., pp. 1–16.

Brink, K. H., Bane, J. M., Church, T. M., Fairall, C. W., Geernaert, G. L., Hammond, D. E., Henrichs, S. M., Martens, C. S., Nittrouer, C. A., Rogers, D. P., Roman, M. R., Roughgarden, J. D., Smith, R. L., Wright, L. D. & Yoder, J. A. 1992 *Coastal Ocean Processes: A Science Prospectus. Rept. No. WHOI-92-18*, Woods Hole Oceanographic Institution, Woods Hole, MA. 103.

Donelan, M. A. 1979 On the fraction of wind momentum retained by waves. In *Marine Forecasting, Predictability and Modeling in Ocean Hydrodynamics* (Nihoul, J. C., ed.), Elsevier, Amsterdam, pp. 141–159.

Eadie, B. J., Schwab, D. J., Leshkevich, G. L., Johengen, T. H., Assel, R. A., Holland, R. E., Hawley, N., Lansing, M. B., Lavrentyev, P., Miller, G. S., Morehead, N. R., Robbins, J. A. & Van Hoof, P. L. 1996 Anatomy of a recurrent episodic event: a winter-spring plume in southern Lake Michigan *EOS. Transactions of the American Geophysical Union* **77,** 337–338.

Foster, D. S. & Colman, S. M. 1992 *Thickness and Distribution of Post Glacial Deposits Beneath Lake Michigan*. US Geological Survey Miscellaneous Field Map, MI-2202.

Galappatti, G. & Vreugdenhil, C. B. 1985 A depth-integrated model for suspended sediment transport. *Journal of Hydraulic Research* **23,** 359–376.

Garcia, M. H. & Parker, G. 1991 Entrainment of bed sediment into suspension. *Journal of Hydraulic Engineering* **117,** 414–435.

Grant, W. D. & Madsen, O. S. 1979 Combined wave and current interaction with a rough bottom. *Journal of Geophysical Research* **84,** 1797–1808.

Hasselmann, K., Barnett, T. P., Bouws, E., Carlson, H., Cartwright, D. E., Enke, K., Ewing, J. A., Gienapp, H., Hasselmann, D. E., Kruseman, P., Merrburg, A., Muller, P., Olbers, D. J., Richter, K., Sell, W. & Walden, H. 1973 Measurements of wind-wave growth and swell decay during the Joint North Sea Wave Project (JONSWAP). *Deutsche Hydrographische Zeitschrift* **A12,** 95.

Liu, P. C., Schwab, D. J. & Bennett, J. R. 1984 Comparison of a two-dimensional wave prediction model with synoptic measurements. *Journal of Physical Oceanography* **14,** 1514–1518.

Lou, J. 1995 *Modelling of Hydrodynamics and Suspended Sediment Transport in Coastal Areas*. Ph.D Thesis, James Cook University, Australia.

Lou, J. & Ridd, P. 1996 Wave-current bottom shear stresses and sediment resuspension in Cleveland Bay, Australia. *Coastal Engineering* **29,** 169–186.

Lou, J. & Ridd, P. 1997 Modeling of suspended sediment transport in coastal areas under waves and current. *Estuarine, Coastal and Shelf Science* **45,** 1–16.

Lou, J., Schwab, D. J. & Beletsky, D. 1999 A model of sediment resuspension and transport dynamics in southern Lake Michigan. *Journal of Geophysical Research* (in press).

Mellor, G. L. & Yamada, T. 1982 Development of a turbulence closure model for geophysical fluid problems. *Reviews of Geophysics and Space Physics* **20,** 851–875.

Mortimer, C. H. 1988 Discoveries and testable hypotheses arising from Coastal Zone Color Scanner imagery of southern Lake Michigan. *Limnology and Oceanography* **33,** 203–226.

Resio, D. T. & Vincent, C. L. 1977 Estimation of winds over the Great Lakes. *Journal of the Waterway, Port, and Coastal Ocean Division, ASCE* **102,** 265–283.

Scavia, D. & Bennett, J. R. 1980 Spring transition period in Lake Ontario - a numerical study of the causes of the large biological and chemical gradients. *Canadian Journal of Fisheries and Aquatic Science* **37,** 823–833.

Schwab, D. J. 1989 The use of analyzed wind fields from the Great Lakes marine observation network in wave and storm surge forecast models. *Preprint Volume of the 2nd International Workshop on Wave Hindcasting and Forecasting.* Environment Canada, Atmos. Env. Service, Downsview, Ont. pp. 257–266.

Schwab, D. J. & Bedford, K. W. 1994 Initial implementation of the Great Lakes Forecasting System: a real-time system for predicting lake circulation and thermal structure. *Water Pollution Research Journal of Canada* **29,** 203–220.

Schwab, D. J. & Beletsky, D. 1998 *Lake Michigan Mass Balance Study: Hydrodynamic modeling project. NOAA Tech. Memo. ERL GLERL-108.* NOAA Great Lakes Env. Res. Lab., Ann Arbor, MI, 53 pp.

Schwab, D. J., Bennett, J. R., Liu, P. C. & Donelan, M. A. 1984 Application of a simple numerical wave prediction model to Lake Erie. *Journal of Geophysical Research* **89,** 3586–3589.

Schwab, D. J. & Morton, J. A. 1984 Estimation of overlake wind speed from overland wind speed: a comparison of three methods. *Journal of Great Lakes Research* **10,** 68–72.

Schwab, D. J., Leshkevich, G. A. & Muhr, G. C. 1992 Satellite measurements of surface water temperature in the Great Lakes: Great Lakes Coast Watch. *Journal of Great Lakes Research* **18,** 247–258.

Strub, P. T., Kosro, P. M. & Huyer, A. 1991 The nature of cold filaments in the California Current System. *Journal of Geophysical Research* **96,** 14743–14768.

Van Rijn, L. C. 1985 *Two-dimensional vertical mathematical model for suspended sediment transport by currents and waves. Rep. S488-IV*, Delft Hydraulics Lab.

Van Rijn, L. C. 1986 Mathematical modeling of suspended sediment in nonuniform flows. *Journal of Hydraulic Engineering* **112,** 433–455.

Van Rijn, L. C. 1989 *Sediment transport by currents and waves. Rep. H461*, Delft Hydraulics Lab.

FIGURE 1. Geometry and bathymetry of Lake Michigan showing 2 km computational grid, metrological stations, and location of mid-lake station in southern Lake Michigan.

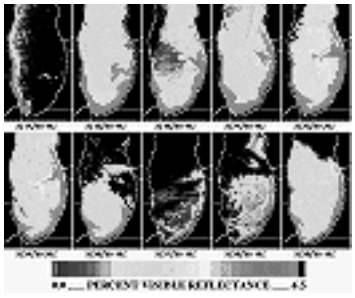

FIGURE 2. Satellite measurements of surface reflectance in southern Lake Michigan.

FIGURE 3. Long term sediment accumulation in southern Lake Michigan (Foster & Colman, 1992). The five ranges of sediment thickness depicted in the map are (from lightest to darkest): 1–2 m, 2–6 m, 6–10 m, 10–14 m, and >14 m. Labelled bathymetric contours are in metres.

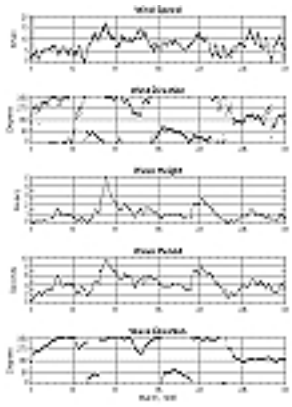

FIGURE 4. Time series of interpolated wind and modelled waves at a location in the centre of southern Lake Michigan for 1–30 March, 1998.

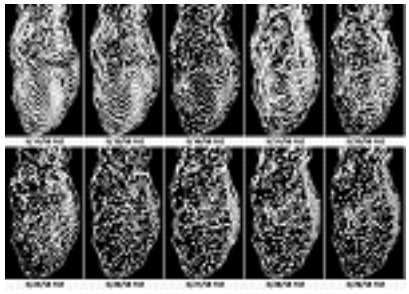

FIGURE 5. Snapshots of particle trajectory animation at times corresponding to satellite images in Figure 2.

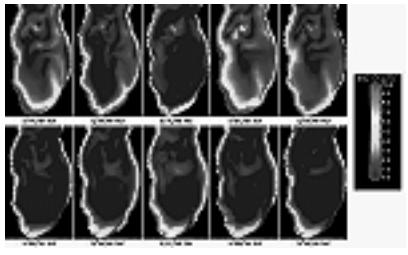

FIGURE 6. Snapshots of suspended sediment concentraiton animation at times corresponding to satellite images in Figure 2.

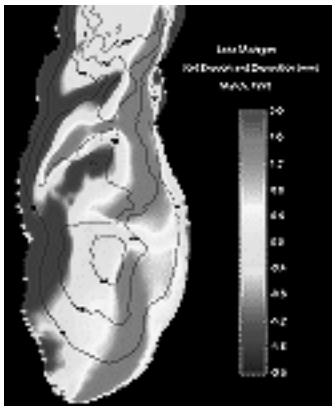

FIGURE 7. Net sediment erosion or depostion calculated from the sediment transport odel during March 1998. The positive values (red) represent depostion, and the negative values (blue) show erosion in mm.

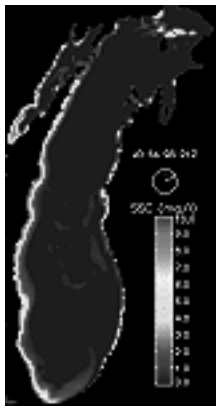

ANIMATION 3. Modelled surface suspended sediment concentration in Lake Michigan for 1–30 March, 1998.

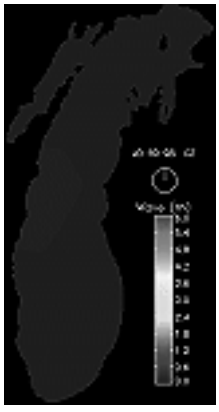

ANIMATION 1. Modelled significant wave height in Lake Michigan for 1–30 March, 1998.

ANIMATION 2. Modelled particle trajectories in Lake Michigan for 1–30 March, 1998.